11 EEG Oscillations and Wavelet Analysis

Christoph S. Herrmann, Maren Grigutsch, and Niko A. Busch

Oscillations in the EEG

Both EEG and ERP measures can be investigated in the frequency domain, and it has been convincingly demonstrated that assessing specific frequencies can often yield insights into the functional cognitive correlations of these signals (Başar et al., 1999).

Analysis of EEG oscillations traces back to the beginning of EEG-based research, when the German neurophysiologist Berger (1929) first observed the dominant oscillations of approximately 10 Hz recorded from the human scalp. Berger coined the term alpha frequency, using the first letter of the Greek alphabet for activity in this frequency range. He dubbed the second type of rhythmic activity that he found in the human EEG as beta, the frequency range of approximately 12–30 Hz. Following this consecutive ordering, Adrian (1942) referred to oscillations around 40 Hz (more general, 30–80 Hz) observed after odor stimulation in the hedgehog as gamma waves. The slow oscillations below 4 Hz, which were discovered next, were labeled delta waves. Finally, waves that cycle 4–8 times per second (4–8 Hz) were named theta oscillations after the first letter of their assumed region of origin, the thalamus (table 11.1).

Evoked versus Induced Oscillations

Oscillations are characterized by their amplitude and phase. The amplitude of an EEG oscillation is typically between 0 and 10 μV. The (cyclic) phase ranges between 0 and 2π. At every point in time one can determine the amplitude and phase of an oscillation. According to a classification of different types of oscillatory activity by Galambos (1992), there are spontaneous, induced, and evoked rhythms, all of which are differentiated by their degree of phase-locking to the stimulus (emitted rhythms in response to omitted stimuli also have been observed, but we will not consider these here). In this framework, spontaneous activity is completely uncorrelated with the occurrence of an experimental condition. Induced activity is correlated with experimental conditions but is not strictly phase-locked to its onset. Evoked activity is strictly phase-locked to

Table 11.1
A list of well-established frequency bands and their names

Frequency	Name
0–4 Hz	Delta
4–8 Hz	Theta
8–12 Hz	Alpha
12–30 Hz	Beta
30–80 Hz	Gamma

the onset of an experimental condition across trials, that is, it has the same phase in every stimulus repetition.

Figure 11.1 (left) illustrates such evoked oscillations, which start at the same time after stimulation in every trial and have identical phases. In this case, the activity is called evoked, it sums, and it is visible in the averaged ERP. However, evoked oscillations are only visible in the ERP to the naked eye if they are of sufficient amplitude. Because high-frequency oscillations usually have lower amplitude than low-frequency oscillations, they are often not visible. Evoked oscillations usually result from any kind of sensory events, such as auditory, visual, or somatosensory stimulation.

If oscillations occur after each stimulation but with varying onset times and/or phase jitter, they are considered as being induced by the stimulus rather than evoked, and are not visible in the averaged ERP. Figure 11.1 (right) illustrates this outcome. One must apply special methods to analyze this type of activity (see below).

Delta and Theta Oscillations

An ERP constitutes a mixture of multiple waves of various frequencies. However, digital filters can selectively show single frequencies while filtering all others out. For example, a bandpass filter lets only a limited range of frequencies pass (see chapter 5 of this volume). When only theta frequencies are admitted (4–8 Hz), for instance, only such slow oscillations will remain in the event-related signal (figure 11.2). Evoked delta and theta oscillations represent the slow potentials in ERPs, such as P300, N400, P600, and so on (Basar-Eroglu et al., 1992). Researchers have described functional correlates of event-related theta oscillations for working memory functions (Tesche & Karhu, 2000; Jensen & Tesche, 2002). Moreover, event-related theta oscillations relating to memory performance have also been shown to interact with faster oscillations in the gamma frequency range (Fell et al., 2003). Note that these event-related signals are not identical to those that one can see with the naked eye in raw EEG, and usually relate to deep sleep (Steriade, McCormick, & Sejnowski, 1993) or malfunctions (Gloor, Ball, & Schaul, 1977).

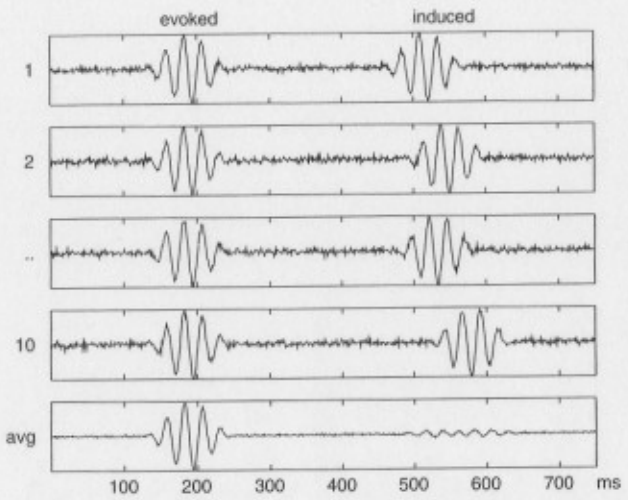

Figure 11.1
If oscillations occur at the same latency after stimulus onset and with the same phase relative to stimulus onset in multiple trials (rows 1–4), they are considered evoked by the stimulus (*left*). If latency or phase jitter relative to stimulus onset, the oscillations are considered to be induced by the stimulus (*right*). Evoked activity sums up in the average (bottom row), whereas induced activity is nearly cancelled out.

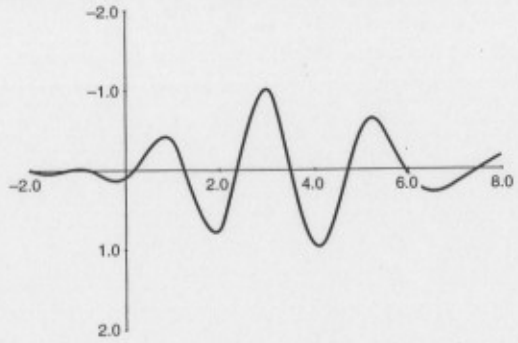

Figure 11.2
EROs in the theta band resulting from applying a 4–8-Hz bandpass filter to an ERP. An event-related theta oscillation emerges after stimulation that then decays over time.

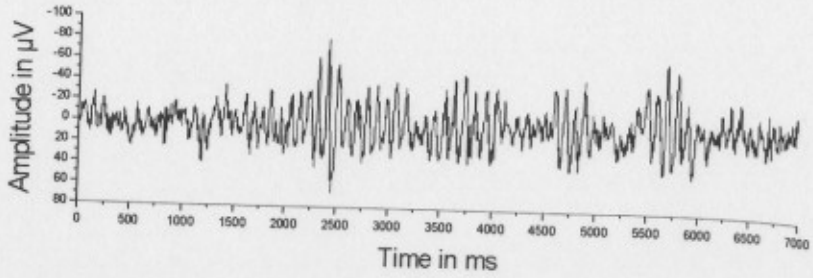

Figure 11.3
Ten seconds of unfiltered, spontaneous EEG showing alpha activity (8–12 Hz).

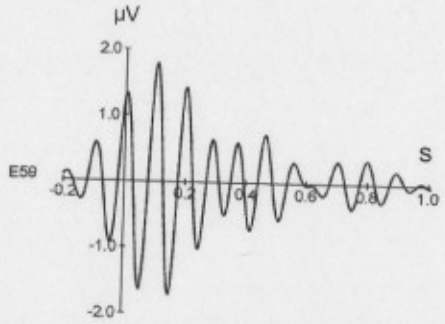

Figure 11.4
Short burst of 10-Hz oscillations evoked by visual stimulation.

Alpha Oscillations

The term alpha oscillation usually refers to the ongoing alpha rhythm. One can observe this rhythm, with approximately 10 Hz, in routine EEG recordings without averaging (cf. figure 11.3). Typically, the amplitude of the 10-Hz rhythm increases and decreases over time, which some have described as waxing and waning. Some authors have even hypothesized that there exist several independent rhythms in the alpha band with different functional properties (e.g., Niedermeyer, 1997). However, this is not the type of alpha activity we want to discuss here. We are interested in 10-Hz oscillations that occur in relation to an experimental condition—that is, evoked or induced 10-Hz oscillations.

Figure 11.4 shows a burst of 10-Hz oscillations after visual stimulation in an occipital electrode (Oz in the 10–20 system). In order to compute this evoked 10-Hz activity, an

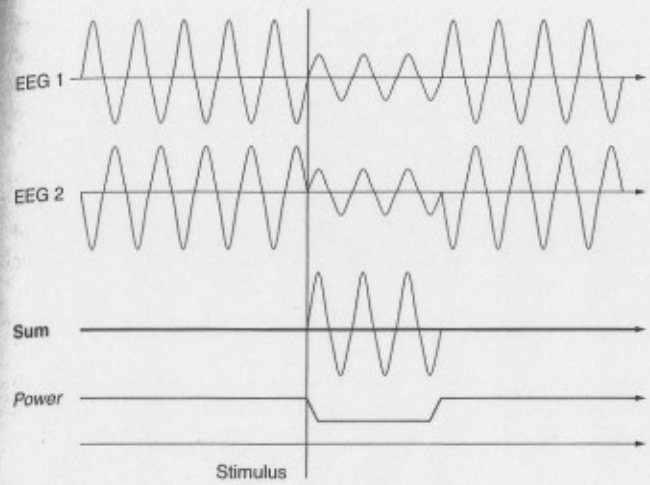

Figure 11.5
A resetting of the phase of alpha oscillations at the time of stimulation leads to a short increase of evoked activity (sum) despite the fact that the amplitude (power) decreases.

ERP was first averaged and then bandpass-filtered in the alpha frequency range. Note that the burst of oscillatory activity seems to start before the onset of stimulation. This is an artifact of the filter algorithm. The filter uses time points of the past and future to compute each time point of the filtered signal. Therefore, the activity "leaks" into past and future events around its real peak (see chapter 5 of this volume).

Most any sensory stimulation—visual, auditory, and somatosensory—can evoke such bursts of alpha activity. The topography of this evoked alpha response is restricted to the primary sensory cortex that was stimulated. Interestingly, this burst of alpha activity is not due to an increase in amplitude. This becomes clear when one computes the total power of alpha activity following a visual stimulus. The total power contains both evoked and induced activity and typically decreases after visual stimulation. Thus, the amplitude of alpha oscillations is reduced after stimulation, whereas the evoked alpha activity is enhanced. Figure 11.5 schematically depicts this phenomenon, called the alpha paradox (Klimesch et al., 1998b). The first two traces show band-pass filtered alpha activity and its amplitude reduction after a visual stimulus. When these traces are simply added up as in the case of an average (third row), only those oscillations that are phase-locked (evoked) remain visible. Due to a so-called phase-resetting, the randomly distributed phase will be reset to start from the same value after stimulation for a short period of time (Brandt, 1997). This leads to the short

burst of evoked alpha activity, because oscillations add up if they have identical phases across trials. However, the behavior of the amplitude is only reflected in the total power measure (bottom row), which is independent of the phase of the oscillations.

Alpha activity has been associated with a large number of cognitive processes. The most important of them are memory processes (Klimesch 1997; Klimesch, Schimke, & Pfurtscheller, 1993), attention (Klimesch et al., 1998a; Yordanova, Kolev, & Polich, 2001), and visual awareness (Sewards & Sewards, 1999; Strüber & Herrmann, 2002). For an overview, see Basar et al. 1997. Although researchers have assumed the generators of EEG alpha activity to reside in cortex, the generators are probably driven by thalamic cells (Steriade et al., 1990; Lopes Da Silva, 1991).

Beta Oscillations

The frequency range from 12 to 30 Hz constitutes the beta frequency band, which has been investigated in the context of motor actions. In particular, beta oscillations are suppressed during motor action but increase (a so-called rebound) approximately one second after movement, with a topography close to the primary sensorimotor regions representing the involved body part (Neuper & Pfurtscheller, 2001). They are also observed during imagined movements and can be elicited by median nerve stimulation (Salmelin & Hari, 1994). During somatosensory stimulation, beta activity is evoked together with gamma and alpha activity (Chen & Herrmann, 2001). Some have assumed that beta oscillations are induced by faster gamma oscillations (Haenschel et al., 2000) and perhaps they in turn induce slower alpha oscillations, a relationship that would explain the presence of all three frequencies in one experimental paradigm. In addition to motor and sensory processes, beta oscillations have also been associated with cognitive processes such as memory rehearsal (Tallon-Baudry, Bertrand, & Fischer, 2001).

Gamma Oscillations

In recent years technical improvements have revealed sensory-evoked oscillations of even higher frequencies. These have been reported up to about 600 Hz (Curio, 1999), the assumed theoretical limit of EEG activity due to the temporal width of single action potentials, which range between 1 and 2 ms. Among high-frequency oscillations, gamma waves (30–80 Hz, cf. figure 11.6) have received a considerable amount of attention because of their important correlates with higher brain functions (Engel, Fries, & Singer, 2001). Some have even assumed that they might be a neural correlate of consciousness (Llinás & Ribary, 1993).

The correlates of processes that are most frequently associated with gamma oscillations are binding phenomena (Müller et al., 1997; Tallon et al., 1995; Tallon-Baudry et al., 1996), perceiving meaningful objects (Keil et al., 1999; Tallon-Baudry et al., 1997), and attention (Tiitinen et al., 1993; Müller, Teder-Sälejärvi, & Hillyard, 1998; Herrmann, Mecklinger, & Pfeiffer, 1999; Herrmann & Mecklinger, 2001; Debener et al., 2003).

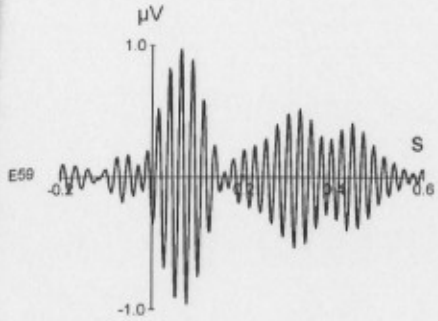

Figure 11.6
Evoked 40-Hz oscillations show a burst shortly after visual stimulation.

Reviews related to the functional relevance of gamma oscillations include Başar-Eroglu et al. 1996b, Tallon-Baudry & Bertrand 1999, Müller et al. 2000, and Herrmann & Knight 2001.

Wavelet Analysis

Frequency Analysis Methods

In principle, every signal can be decomposed into sinusoidal oscillations of different frequencies. Such decomposition is usually computed using the Fourier transform to quantify the oscillations that constitute the signal (Dumermuth, 1977).

There are several methods to exclusively extract oscillations of a specific frequency from ERP data. Among the most popular are filtering, Fourier transformation, and wavelet analysis.

Figure 11.7 shows the results of these three methods to extract frequency information from an ERP. In the left panel, filtering two ERPs with a bandpass filter (35–45 Hz) shows a clear burst of 40-Hz activity around 100 milliseconds. This oscillatory activity is enhanced for the dotted as compared to the solid condition. The middle panel shows Fourier spectrum analyses of the two ERPs. An increase of activity for the dotted condition can be noticed around 40 Hz. However, it is unclear at what point this difference between conditions occurs. The right panel shows the absolute values of the wavelet coefficients of the ERP for a 40-Hz wavelet. The difference between conditions is very prominent and can be observed at every point in time due to the lack of oscillations in

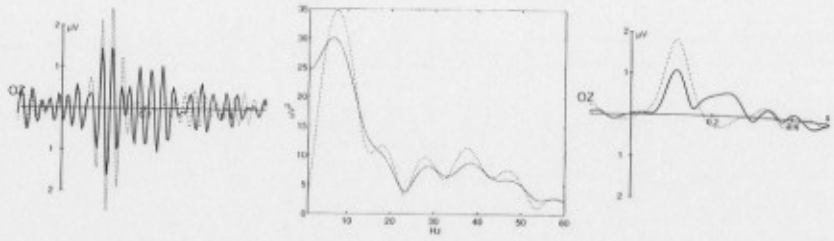

Figure 11.7
Three possibilities to extract frequency information from ERP data: two 35–45 Hz filtered ERPs (*left*), two FFT spectra of the ERPs (*middle*) and the wavelet transforms of the ERPs (*right*). Note that only the filtered signal and the wavelet transform still represent changes over time. The FFT spectra show the entire frequency range but no temporal information.

the signal. One can think of the wavelet transform as the envelope of the bandpass-filtered ERP. The wavelet transform is advantageous over the FFT, because the time course of frequency information can be observed. Although this is also true for the filtered signal, the wavelet transform directly yields the amplitude and the phase of the signal oscillations in the analyzed frequency band when one uses a complex wavelet function. The wavelet amplitude has only positive values and does not bear the problem that oscillations might cancel out when averaging across multiple subjects (negative values in figure 11.7 result from a baseline correction making the wavelet transform a relative measure with respect to the prestimulus interval). Samar et al. (1999) gives a review of using wavelets for EEG analysis.

The Wavelet Transform

To compute a wavelet transform, the original signal time series, $x(t)$, is convolved with a scaled and translated version of a mother wavelet function, $\psi(t)$. The convolution leads to a new signal of wavelet coefficients,

$$W_x^{\Psi}(b,a) = A_{\Psi} \cdot \int \Psi^* \left(\frac{t-b}{a} \right) \cdot x(t) \cdot dt$$

where Ψ^* denotes the complex conjugation of the wavelet function, b is the translation parameter, a is the wavelet's scaling parameter, and A_{Ψ} denotes a (wavelet-specific) normalization parameter. The wavelet coefficients quantify the similarity between the original signal and the wavelet function at a specific scale a and target latency b. Hence, the wavelet coefficients depend on the choice of the mother wavelet function.

The mother wavelet is constructed in such a way that it has zero mean and is localized in both time and frequency space. This is in contrast to the Fourier transform,

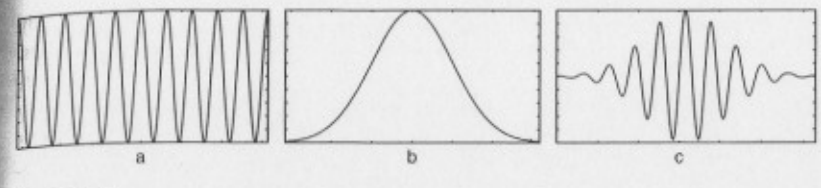

Figure 11.8
Multiplying a sinusoidal function (*a*) and an envelope function (*b*) results in a wavelet (*c*).

where the harmonic basis functions have a well-determined frequency but extend over the entire time axis. Due to its localization properties, the wavelet transform allows one to follow the time course of component structures in the signal. This feature is of crucial importance when analyzing nonstationary signals, but has to be paid for with a reduced frequency resolution.

Another important feature of the wavelet transform is its zooming property. Varying the scaling parameter, a, from high to low values, compresses the wavelet function, $\psi(|t-b|/a)$. The corresponding wavelet transform zooms from coarser (i.e., low-frequency) to finer (i.e., high-frequency) signal structures.

In the case of Morlet's wavelets, also referred to as Gabor wavelets, the mother wavelet function is given by the formula

$$\Psi(t) = e^{j\omega_0 t} \cdot e^{-t^2/2}$$

where j denotes the imaginary unit, $(-1)^{1/2}$, and ω_0 is 2π times the frequency of the unshifted and uncompressed mother wavelet (if fewer than six cycles of a wavelet are used, a correction term $e^{-\omega_0/2}$ has to be subtracted from $e^{j\omega_0 t}$ to guarantee that the wavelet still has a mean value of zero). Morlet wavelets are complex functions. Both their real and imaginary parts consist of a harmonic oscillation windowed in time by a Gaussian envelope. Figure 11.8 illustrates this schematically.

Using sinusoidal wavelets such as the Morlet wavelet is ideally suited for detecting sinusoidal EEG activity, because the wavelet transform is similar to detecting whether the signal contains the used wavelet. Other wavelets that are more spiky can be used for detecting transient phenomena in EEG such as epileptic spikes (Schiff et al., 1994).

In the frequency domain, Morlet wavelets also have a Gaussian shape around their modulation frequency, that is, the wavelet scale can be directly interpreted in terms of a well-defined center frequency (we will use the terms scale and frequency synonymously here). Hence, we can write the scaled, unshifted wavelet as a function of frequency, f:

$$\Psi(t,f) = e^{j2\pi f t} \cdot e^{-t^2/2\sigma_t^2}$$

where the standard deviation σ_t of the Gaussian temporal envelope is reciprocally related to the frequency ($\sigma_t \sim 1/f$) in order to retain the wavelet's scaling properties. By this scaling one obtains the same number of significant wavelet cycles, $n_{co} = 6\sigma_t f$, at all frequencies. The standard deviation in the frequency domain is given by $\sigma_f = (2\pi\sigma_t)^{-1}$. It grows proportionally to the modulation frequency—that is, σ_f/f is constant. This implies that the Morlet wavelet transform has a different time and frequency resolution at each scale. If the number of significant cycles of the wavelet is kept constant, it varies in temporal width as a function of frequency, because the same number of cycles spread over a longer interval for lower frequencies. Therefore, at high frequencies the temporal resolution of a wavelet is better than at low frequencies. However, the inverse is true for the frequency resolution of the wavelet transform. At low frequencies the wide temporal extension of the wavelet results in a good frequency resolution, because the analysis considers many time points. At high frequencies, where the small width leaves fewer time points, the frequency resolution decreases. Figure 11.9 illustrates this.

In addition to this general trade-off between temporal and frequency resolution, wavelets also allow one to adjust their temporal and frequency width for any given center frequency. By using a wavelet with more cycles (i.e., larger n_{co}) the frequency resolution increases, because the frequency can be determined via more time points—but of course, the temporal resolution decreases at the same time. Using fewer cycles has the opposite effect.

Convolutions with Morlet wavelets can be computed for multiple frequencies in order to yield a time-frequency (TF, cf. figure 11.16) representation of the analyzed signal, $x(t)$. Because the Morlet wavelet function is complex, the wavelet transform, $W_x(t, f)$, is also a complex function that can be divided into its real part, $\Re\{W_x\}$, and its imaginary part, $\Im\{W_x\}$. Alternatively, using the polar notation, $W_x = |W_x| \exp\{j\theta_x\}$, the wavelet coefficients can be described by an amplitude, $|W_x| = [\Re\{W_x\}^2 + [\Im\{W_x\}^2]^{1/2}$, and a phase angle, $\theta_x(t, f) = \tan^{-1}[\Im\{W_x\}/\Re\{W_x\}]$.

One can think of a wavelet function as a finite impulse response filter. In this context, the real part, $\Re\{W_x\}$, of the Morlet wavelet transform represents a bandpass-filtered signal, $x_f(t)$, whereas the imaginary part, $\Im\{W_x\}$, yields a 90-degree phase shifted signal (Hilbert transform). The amplitude, $|W_x(t, f)|$, corresponds to the envelope of the filtered signal, $x_f(t)$. It quantifies the instantaneous oscillatory strength of the signal with respect to the analyzed frequency band. Figure 11.10 shows a time-frequency representation of the signals depicted in figure 11.1. The TF representation has been obtained by gray-scale coding of the wavelet amplitudes. Positions on the horizontal axis correspond to different latencies, whereas different wavelet center frequencies have been mapped to the vertical axis.

In analogy to the Fourier power spectrum, the wavelet power spectrum is defined as $|W_x(t, f)|^2$. It is a measure for the signal energy (signal variance) contained in the time-

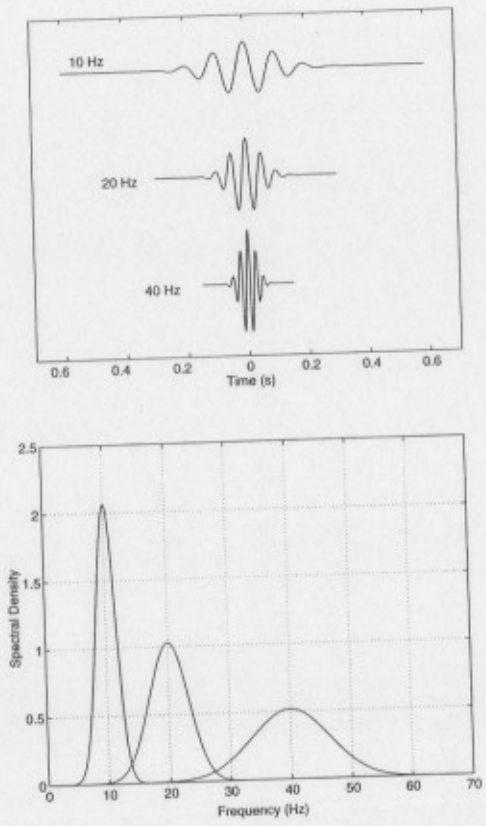

Figure 11.9
Three Morlet wavelets (*top*, only real part shown) with different central frequencies and the corresponding frequency spectra (*bottom*). A low-frequency wavelet of 10 Hz is very broad in the time domain but has a good frequency resolution, picking up only activity from adjacent frequencies in a wavelet analysis (left peak in frequency spectrum). A wavelet with a frequency of 40 Hz is more localized in time but has a lower frequency resolution, picking up frequencies from a wider range in a wavelet analysis (right peak in frequency spectrum).

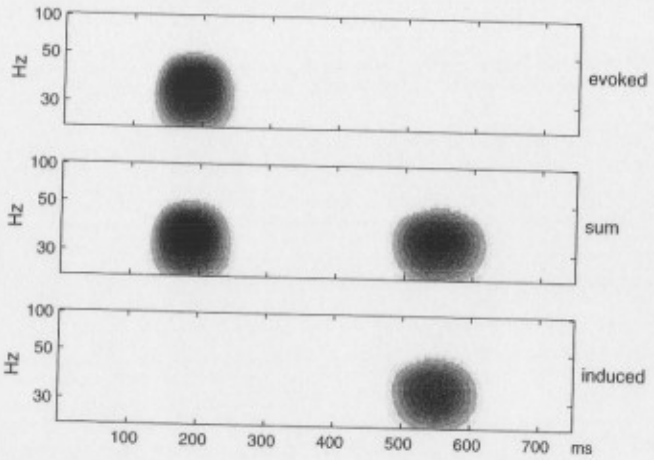

Figure 11.10
Multiple convolutions can be mapped in a time frequency representation. This is shown for the evoked gamma activity (*top*) of the example in figure 11.1, the sum of evoked and induced gamma activity (*middle*) and isolated induced gamma activity (*bottom*). The induced activity has been estimated by the difference of total and evoked activity.

frequency bin covered by the transform, centered around time point t and frequency f. The wavelet functions can be normalized prior to the convolution to have unit energy at all scales. In this case, the wavelet power spectra of an analyzed signal are then directly comparable to each other across all scales. For the Morlet wavelet transform this normalization is achieved with the factor $A_\psi = \sigma_t^{-1/2}\pi^{-1/4}$.

If, however, the wavelet transform should directly yield the amplitude of the analyzed signal, one needs to use a different normalization factor. The Morlet wavelet transform is very similar to the Gabor transform (windowed Fourier transform). The main difference is that in the wavelet method, the width of the data window is not fixed but adapted to the analyzed frequency. In analogy to the Gabor transform, the wavelet amplitude spectrum, $|W_x(t, f)|$, yields the instantaneous amplitude of an oscillation when using the Gabor normalization factor A_ψ:

$$A_\psi = \sigma_t^{-1}(2/\pi)^{1/2}$$

To represent phase-locked (evoked) activity in an ERP experiment, the wavelet transform is computed on the average over the single trials (i.e., on the ERP):

$$\text{Evoked} = \left| A_\Psi \int \Psi^* \left(\frac{t-b}{a} \right) \cdot \frac{1}{N} \sum_{i=1}^{N} eeg_i(t)\, dt \right|$$

Note that absolute value (or absolute power) is calculated. After calculating the evoked activity, the frequency-specific baseline activity can be subtracted to yield values that indicate oscillatory amplitude (or power) relative to baseline.

When wavelet transforms are computed, the convolution peaks at the same latency as the respective frequency component in the raw data, although the peak width will be smeared. Therefore, the baseline should be chosen to precede the stimulation by half the width of the wavelet (e.g., 75 ms for six 25-ms cycles of a 40-Hz wavelet) to avoid the temporal smearing of poststimulus activity into the baseline. To avoid distortions by the rectangular window function that can result from "cutting out" a single epoch from continuous raw data (edge effects), the convolution should start and end one-half of the wavelet length before the baseline and after the end of the assessed time interval, respectively.

The TF representation of the ERP contains only that part of the activity that is phase-locked to the stimulus onset. To compute the activity that is not phase-locked to stimulus onset (and is therefore cancelled out in the average), one can compute the total activity (sum of evoked and induced activity). To calculate the sum of all activity at one frequency, average the absolute values of the wavelet transforms of the single trials, which means that each single trial is at first transformed and the absolute values (or alternatively the power values) are averaged subsequently:

$$\text{Total} = \frac{1}{N} \sum_{i=1}^{N} \left| A_\Psi \int \Psi^* \left(\frac{t-b}{a} \right) \cdot eeg_i(t)\, dt \right|.$$

The corresponding TF representation (sum) contains all activity of one frequency that occurred after stimulus onset, no matter whether it was phase-locked to the stimulus or not (cf. figure 11.10). As above, the activity in a prestimulus interval can be subtracted to obtain a relative measure.

Necessary Conditions for Recording Oscillations

The analysis of EEG frequencies requires some precautions when data are recorded. We discuss these next.

Hardware Requirements

Two parameters of the recording equipment are critical for properly recording oscillatory activity. (1) The sampling rate has to be set to a value that is at least twice the highest frequency that should be analyzed (four times is better, and is required by some software). For example, to analyze gamma activity up to 80 Hz, one needs a minimum sampling rate of 160 Hz, and 320 is recommended. (2) The low-pass filter needs to be set to a value higher than the highest frequency that should be analyzed. The low-pass filter is usually integrated in the analog amplifier to prevent aliasing

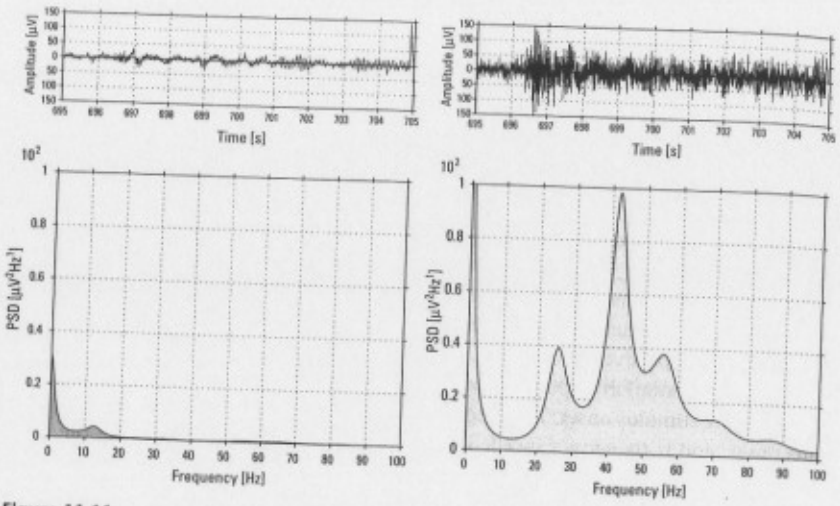

Figure 11.11
Clean EEG data and its frequency spectrum (*left*) and an epoch with EMG contamination leading to frequency peaks around 40 Hz.

errors when digitizing analog data. This step is sometimes overlooked when trying to record high-frequency oscillations for the first time.

Artifact Rejection

All artifacts that contaminate traditional ERP averages should be excluded from frequency analysis. In addition, there are several specific artifact conditions that are especially crucial when analyzing oscillatory activity.

When analyzing alpha activity, subjects should keep their eyes open even if they have no visual task to perform. When they close their eyes, strong alpha oscillations will appear in the EEG that show no correlation with the cognitive task and contaminate the analysis.

A potential confound of human gamma activity is electromyography (EMG). If subjects sit uncomfortably or chew during an EEG session and innervate their muscles, the EEG electrodes will record EMG activity. This high-frequency muscle-related activity (30–80 Hz) can be mistaken for gamma EEG activity. Therefore, all epochs that are subsequently averaged should be visually evaluated for the presence of such EMG artifacts, which should then be excluded from further analysis.

Figure 11.11 shows 10 s of clean EEG and the corresponding frequency spectrum with a 0-Hz and a 12-Hz alpha peak (left). EMG activity can easily be detected in the time domain (right) but may be mistaken for gamma activity in the spectrum.

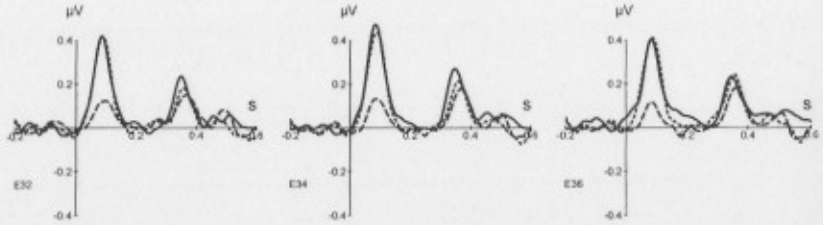

Figure 11.12
Evoked gamma responses in response to visual stimuli of different size. Large (solid) and medium (dotted) stimuli evoke strong gamma peaks, whereas small (dashed) stimuli evoke only weak responses.

Stimulus Size

Exogenous parameters such as physical stimulus properties influence the amplitude of sensory evoked potentials. The same dependence upon exogenous parameters can be observed for oscillatory EEG activity. Especially for low-amplitude activity in the gamma range, it is crucial to present stimuli of sufficient size in order to evoke reliable responses. Cognitive differences between experimental conditions can only be observed when the amplitude is sufficiently high.

Figure 11.12 shows how the evoked gamma response depends upon stimulus size. Large (9° vis. angle) and medium (5° vis. angle) stimuli evoked gamma peaks of approx. 0.4 μV over occipital cortex that clearly differ from baseline activity. Small (1° vis. angle) stimuli, however, evoke only weak gamma responses that are only twice the amplitude of the baseline noise. The first peak of gamma activity is due to the onset of the visual stimuli and the second one due to their offset.

Stimulus Duration

Due to the fact that stimulus onsets as well as stimulus offsets evoke significant gamma bursts, the duration of a stimulus plays an important role in the observed pattern of oscillations.

When stimuli are sufficiently long in duration, their offset responses can clearly be differentiated from their onset peaks. Figure 11.13 illustrates this for stimuli of 250-ms duration (solid) and 150-ms duration (dotted). If, however, the duration is very short, onset peak and offset peak mix into each other and cannot be distinguished (50-ms duration, dashed). This is also true for ERP analysis, but is often disregarded. When analyzing late ERP components they should not be contaminated by offset responses.

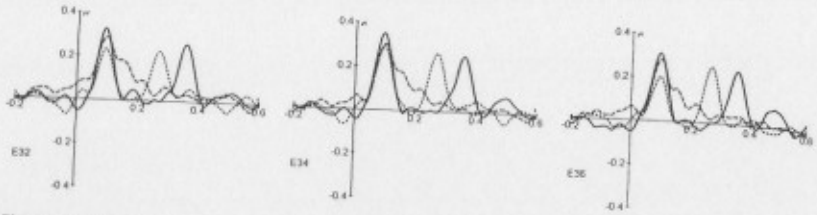

Figure 11.13
Stimuli of three different durations evoke approximately the same onset peak of gamma activity around 100 ms but different offset peaks. Stimulus durations: 250 ms (solid), 150 ms (dotted), and 50 ms (dashed).

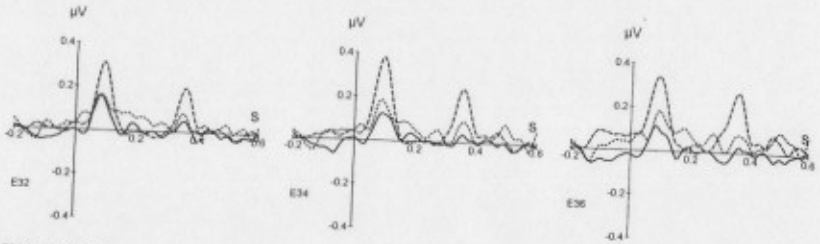

Figure 11.14
Influence of eccentricity on the evoked gamma response. Centrally presented stimuli (dashed) evoke much larger responses than stimuli of identical size and shape that are presented more eccentrically (dotted and solid).

Stimulus Eccentricity

Gamma oscillations are mainly generated over sensory cortices. In case of the visual cortex, the central visual field is represented by a greater number of neurons than the peripheral visual field. This leads to an influence of the eccentricity of visual stimuli on the evoked gamma response.

Figure 11.14 shows the responses to three identical stimuli at different eccentricity. A centrally presented stimulus (dashed) leads to the largest response. Already at 4 degrees eccentricity (dotted) the response is much lower. At an eccentricity of 8 degrees, it is even lower. Therefore, it is advantageous if one can apply central presentation.

Age of Subjects

Age influences the amplitude of ERPs (Polich, 1997). The same is true for evoked oscillations, especially in the gamma frequency range. Already at an age of around 45 years the amplitude of the response begins to decrease (Böttger, Herrmann, & von Cramon, 2002). Therefore, subjects must be chosen such that they represent a homogeneous age. Otherwise age might be a confound for cognitive parameters.

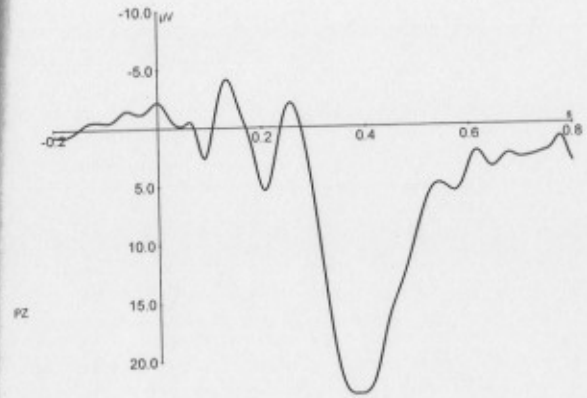

Figure 11.15
An ERP in response to a visual target stimulus exhibiting a series of components: P1, N1, P2, N2, and P3.

Analysis of an ERP

When all technical aspects have been taken care of, interesting new findings can be observed in the oscillatory EEG responses. As Makeig et al. (2002) nicely demonstrated, an ERP (figure 11.15) and the frequency representation of the ERP (figure 11.16) are two alternative ways of investigating the EEG in response to experimental stimulation.

Figure 11.16 shows the alternative representation of the ERP in figure 11.15 as a time-frequency plot. The early ERP components are visible as high-frequency blobs in the gamma and beta range, and the later components are visible as two overlapping big blobs in the theta and delta range. The earliest frequency component around 36 Hz has the shortest duration and terminates around 100 ms after stimulation. The subsequent oscillation around 18 Hz is already more widely spread across time and lasts approximately 150 ms after stimulation. The theta wave of about 7 Hz remains active until around 350 ms and a delta wave (approx. 3 Hz) can be observed up to 700 ms poststimulus. Such a shift from early high-frequency components to later low-frequency components is a typical finding (Chen & Herrmann, 2001; Haenschel et al., 2000). Sometimes they reveal a frequency relation of 4:2:1, suggesting underlying neural resonance circuits that trigger each other (Herrmann, 2001).

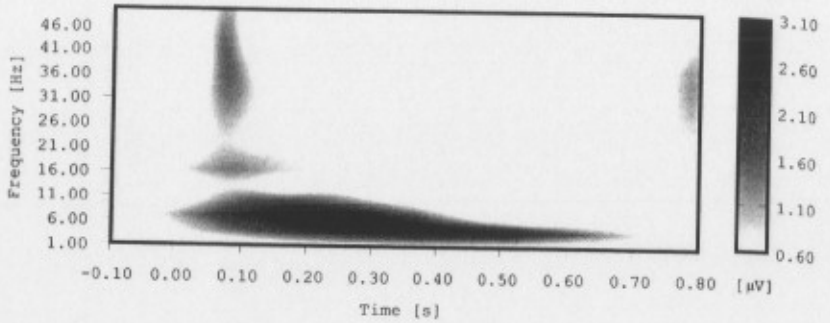

Figure 11.16
The time-frequency representation of the ERP in figure 11.15.

Wavelet-Based Dynamic Interdependence Measures

In the neuroscience community there has been growing interest not only in the modularization of brain functions (i.e., the functional specialization of local brain areas), but also in the cooperation between specialized and widely distributed areas that are a prerequisite of higher cognitive functions and large-scale integration. Such cooperation requires a certain degree of dynamic synchronization between the involved neuronal assemblies that in turn should be reflected in the EEG as a dynamic interrelation between the measured brain signals (von Stein et al., 1999; Schack et al., 1999).

Classical interrelation measures such as Fourier-based coherence and correlation depend on the stationarity of the measured signals, which is rarely fulfilled with concurrent brain signals. Recently, alternative tools based on wavelet analysis have been developed and successfully applied to EEG/MEG signals (e.g., Lachaux et al., 2002). They allow one to track the time course of coherence in nonstationary neuronal signals with good temporal and frequency resolution.

Wavelet Coherence

Analogous to classical coherence, wavelet coherence is defined as the cross-wavelet spectrum of two signals, x and y, normalized by their corresponding autospectra:

$$coh_w(t, f) = \frac{|W_{xy}(t, f)|}{\sqrt{W_{xx}(t, f) \cdot W_{yy}(t, f)}}$$

where $W_{xy}(t, f)$ is the cross-wavelet spectrum (see below) at latency t and frequency f, whereas W_{xx} and W_{yy} denote the auto-spectra of x and y, respectively. Wavelet coherence ranges between 0 and 1. It is a measure of the degree of linear relationship

between x and y in a specific time-frequency bin. The instantaneous cross-wavelet spectrum can be estimated from the product of the corresponding univariate wavelet coefficients, $W_{xy}(t, f) = W_x(t, f) \cdot W_y^*(t, f)$. As is the case with Fourier cross-spectra, this estimate is inconsistent and has to be smoothed in an appropriate way in order to improve reliability.

In an event-related potential paradigm, the smoothing can be done across trials:

$$W_{xy}(t, f) = \frac{1}{N} \sum_{k=1}^{N} W_x^k(t, f) \cdot W_y^{k*}(t, f)$$

where N is the total number of trials and W^k means the wavelet coefficient calculated from a signal recorded during the kth trial. This method yields a coherence measure that is very similar to the event-related coherence introduced by Rappelsberger, Pfurtscheller, and Filz (1994). It does not require stationarity across time but is based on the (also questionable) assumption of stationarity across trials.

The wavelet coherence method introduced by Lachaux et al. (2002) estimates W_{xy} by averaging over a time period around the target latency,

$$W_{xy}(t, f) = \frac{1}{\delta} \int_{t-\delta/2}^{t+\delta/2} W_x(\tau, f) \cdot W_y^*(\tau, f)\, d\tau$$

Using Morlet wavelets, this approach corresponds to the WOSA (Welch overlapping segment averaging) estimate of the cross-spectrum (Welch, 1967), with the exception that, in the wavelet-based method, the length of the smoothing window can be varied in dependence upon the target frequency, f. The smoothing window can be chosen to contain the same fixed number of cycles, n_{cy}, at all frequencies, that is, $\delta = n_{cy}/f$. Due to the flexible integration window, the wavelet coherence measure yields a more consistent time-frequency resolution than the WOSA method. Moreover, the same statistical performance of the coherence estimator can be achieved at all frequencies. Bias and variance of the wavelet coherence estimator have been shown to depend only on the number of independent data epochs entering into the calculation of coherence (Lachaux et al., 2002). The ratio n_{cy}:n_{co} gives the number of independent (nonoverlapping) data segments, where n_{co} denotes the number of significant wavelet cycles. In order to gain statistical power, this ratio should be chosen as high as possible. However, a large n_{cy} (i.e., a large integration window) diminishes the temporal resolution for measuring coherence and decreases the probability of detecting short-lasting coherent epochs. Therefore, n_{cy} should be adapted to the length of the coherent epochs being searched for, using larger integration windows for longer epochs of coherency. By contrast, the parameter n_{co} has influence on the frequency resolution of the wavelet transform and thus, on the frequency selectivity of the coherence measure, which decreases for low values of n_{co}. Hence, n_{co} must be chosen in accordance to

the frequency range of interest. Typical values Lachaux et al. (2002) proposed are $n_{co} \geq 3$ for wide frequency bands (more than 10 Hz) and values up to 8–10 for narrow bands.

Phase Synchronization

Coherence does not separate the effects of covariance of the amplitude waveforms and of the phases of two oscillatory signals. The recently developed concept of phase synchronization of chaotic (and/or noisy) systems (Rosenblum, Pikovsky, & Kurths, 1996) is more general. It implies the appearance of a certain relationship between the phases of oscillatory (sub)systems, but does not impose restrictions on their irregular amplitudes, which may remain noncorrelated. This concept is based on the well-known fact that weak coupling first affects the phases of oscillators, not their amplitudes. Hence, the detection of phase synchronization should be sufficient in order to reveal an interaction between two weakly coupled (sub)systems.

With respect to brain signals, phase synchronization in certain frequency bands is supposed to be a central mechanism in neuronal information processing (Varela et al., 2001). Based primarily on animal experiments, there is evidence that synchronization of neuronal activity within sensory cortex is involved in feature binding (Eckhorn et al., 1988; Gray et al., 1989). Transient synchronization between physically distant brain areas has also been reported (Roelfsema et al., 1997). This suggests a possible mechanism for large-scale integration, establishing a dynamic link between neural assemblies by temporarily adjusting their discharge frequencies. Recent experimental results from intracranial and scalp recordings support the assumption that magnitude and phase of brain signals might indeed be involved in a different manner during a cognitive process (Rodriguez et al., 1999; Bruns et al., 2000).

Instantaneous Phase Difference The parameter for measuring phase synchronization is the relative phase angle between two oscillatory systems. Neuroelectrical recordings are broad-band signals and their phase cannot thoroughly be defined. Formally, one could apply the analytic signal approach (Gabor, 1946) and assign an instantaneous phase and an instantaneous amplitude via the Hilbert transform. However, the Hilbert phase and Hilbert amplitude have direct physical meaning only for band-limited signals.

As an alternative, the Morlet wavelet transform acts as a bandpass filter that, at the same time, yields separate values for the instantaneous amplitude $a(t, f)$ and the phase $\theta(t, f)$ of a time-series signal at a specific frequency f. Thus, the wavelet phases of two neuronal signals x and y can be utilized to determine their instantaneous phase difference in a given frequency band

$$\Delta\theta(t, f) = \theta_x(t, f) - \theta_y(t, f)$$

and to establish a synchronization measure that quantifies the coupling of phases independent from amplitude effects. (Note that according to the above equation, the phase difference has to be calculated from the unfolded univariate phase angles.)

Transient phase entrainment (phase locking) is observed if the phase difference remains approximately constant over some time period (typically hundreds of milliseconds in the context of neurocogniton). Due to the noisy and/or chaotic nature of neuronal signals, their relative phase is usually not bounded even when there exists some phase coupling between them. For weak noise, the phase difference fluctuates around some mean phase shift with occasional rapid phase jumps of $\pm 2\,\pi$. For strong and unbound noise (i.e., Gaussian noise), these phase slips occur irregularly. That means that phase locking can be detected in a statistical sense only (Tass et al., 1998; Rosenblum et al., 2001). One has to analyze the distribution of the relative phase angles on the unit circle (wrapped to the interval $[0, 2\pi]$). For independent signals, this distribution will be close to uniform, whereas synchrony shows up as the appearance of a dominating peak.

Figure 11.17 shows the phase difference between the 8-Hz oscillations recorded at electrodes O1 and F9 after visual stimulation. Although the phase difference varies over time before stimulation, it remains stable at a value of approx. $0.83\,\pi$ (2.6 rad) after stimulation for about 250 ms, as the plateau of the curves shows.

Phase-Locking Statistics Researchers have proposed different synchronization measures based, for example, on the Shannon entropy, mutual information, a stroboscopic approach, or directional statistics (for reviews, see Tass et al., 1998; Rosenblum et al., 2001). According to directional statistics (Mardia & Jupp, 2000), the coherence of an angular distribution θ_i can be quantified by estimating the phase-locking index (PLI),

$$PLI = |\langle e^{i\theta} \rangle| = \sqrt{\langle \cos\theta \rangle^2 + \langle \sin\theta \rangle^2} = 1 - CV$$

where brackets denote the expectation operator and CV is the circular variance. It is easy to confirm that the PLI ranges between zero for uniformly scattered phases and one in the case of perfect phase locking.

In a repeated-stimulus design, one can estimate the PLI by averaging over trials (Lachaux et al., 1999):

$$PLI(t, f) = \frac{1}{N}\left|\sum_{k=1}^{N} \exp\{j\Delta\theta^k(t, f)\}\right|$$

where N is the total number of trials and $\Delta\theta^k$ represents the instantaneous phase difference of the two brain signals recorded during the kth trial. The bivariate PLI measures the intertrial variability of the frequency-specific relative phase of two brain

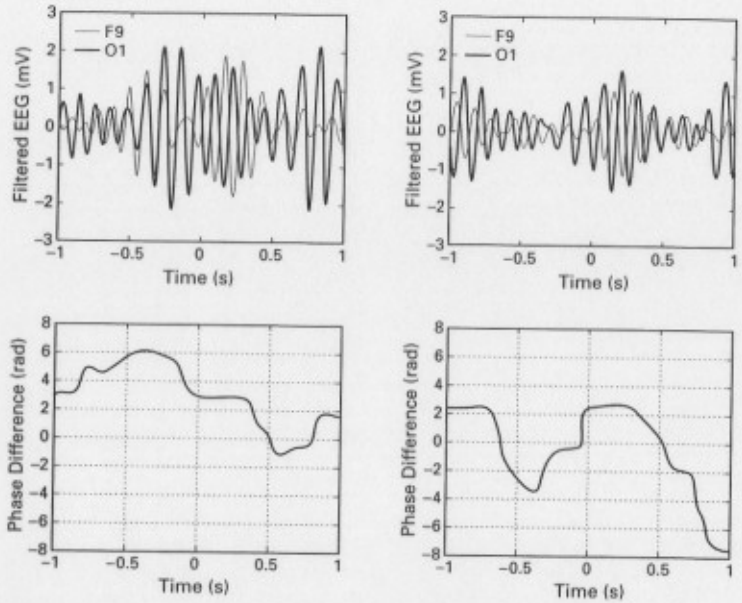

Figure 11.17
Two time courses of 8-Hz event-related oscillations after wavelet decomposition for two electrodes (*top*). The phase differences (*bottom*) reveal that after stimulation (at 0 ms) there is a stable phase relation between the two electrodes in both trials from 0 to approx. 250 ms.

signals at a given target latency—that is, it quantifies the stability of a linear phase relationship across trials.

Figure 11.18 shows the TF representation of the intertrial PLI for two EEG scalp recordings in a visual ERP experiment. A prominent epoch of transient phase coherence is detectable shortly after stimulus onset. The phase locking confines selectively to the alpha band.

Figure 11.19 shows how an experimental stimulus influences the phase of an oscillation. Before visual stimulation, the phase differences between the 8-Hz oscillations in electrodes O1 and F9 were almost randomly distributed (left panel). After a visual stimulus occurred, however, most phase differences showed a value of 150 degrees. This indicates that the stimulus affects the phase of the oscillations.

The PLI measure offers a good temporal resolution, limited only by the width of the wavelet function applied for the univariate phase estimation. Due to the trade-off be-

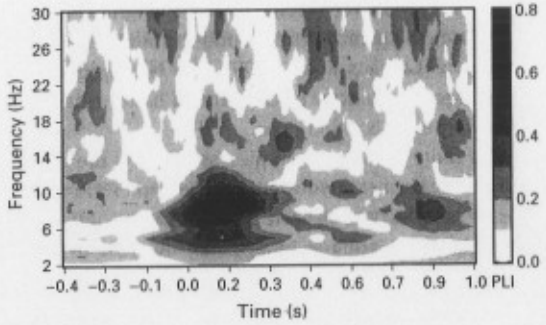

Figure 11.18
TF representation of the bivariate intertrial PLI estimated from two simultaneous EEG recordings (from an occipital [O1] and a frontal scalp electrode [F9]) during visual stimulation of a human subject (stimulus onset at time $t = 0$; $N = 59$ trials; $n_{co} = 6$ significant wavelet cycles). After stimulus onset, a transient period of phase coherence is selectively detected in the alpha band.

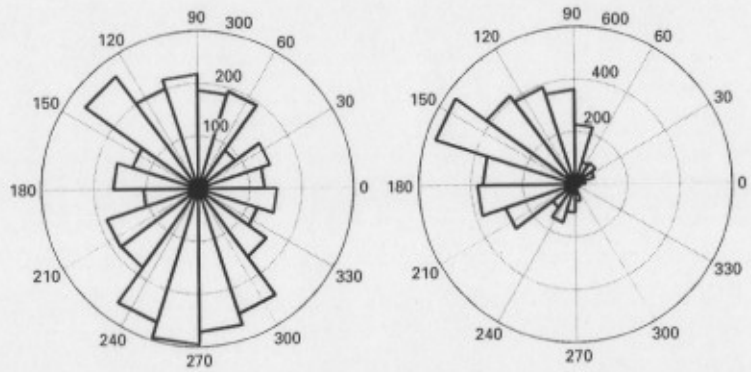

Figure 11.19
The phase distribution of the phase differences of the 8-Hz oscillations between electrodes O1 and F9. The numbers on the circle denote the phase difference in degrees and the extension of a wedge indicates how many single trials showed this phase difference. Before visual stimulation the phases were randomly distributed (*left*). In a time interval from 50 to 300 ms after stimulation the phases were clustered around a value of about 150 degrees (0.83π, *right*).

tween temporal and frequency resolution of the wavelet transform, it might be advantageous to prefilter the signals in a narrow frequency band around the target frequency prior to estimating their wavelet phases (Lachaux et al., 1999). This is recommended especially when dealing with high target frequencies in the gamma band, where the frequency resolution of the wavelet transform is rather poor.

When one estimates the PLI from a finite number of samples, as is always the case in real situations, a nonzero PLI value will be measured even if the samples are drawn from a uniform distribution. For N samples, the expected PLI value (i.e., the bias) is $N^{-1/2}$. One can apply the Rayleigh test (Mardia & Jupp, 2000) in order to assess significance of the detected phase locking against the null hypothesis of a uniform distribution.

Because the sampling distribution of the statistics is usually unknown for brain signals, Lachaux et al. (1999) have proposed a Monte Carlo approach based on the shuffling of trials. Surrogate values are computed from the same signals x and y used for original PLI estimation, except that the order of trials for y is permuted before calculating the relative phases. That means that the instantaneous phase difference is computed from signals that have been recorded during different trials and can thus be considered to be uncorrelated. For each permutation, the maximum PLI value is measured and compared against the original PLI value. The percentage of surrogate values that are greater than the original PLI at a given latency is called phase-locking statistics (PLS) (Lachaux et al., 1999). For PLS values that are smaller than a chosen significance level, the measured synchrony is considered significant. The number n of permutations needed for PLS calculation depends on the chosen significance level p; for a one-sided test it is given by $n = 1/p - 1$ (Theiler et al., 1992; Schreiber & Schmitz, 2000).

Although PLS is a powerful method, it has its caveats. Note that PLS fails to reject the null hypothesis in the important case when both univariate signals have constant phases across trials and thus, the bivariate phases are perfectly locked (Lachaux et al., 1999). PLS also cannot be applied to single trials (or averaged signals such as ERPs). Moreover, it fails to detect periods of synchrony that occur with varying phase delay across trials or at jittering latencies. As an alternative, Lachaux et al. (2000) proposed the single-trial phase-locking index

$$S - PLI(t, f) = \frac{1}{\delta}\left|\int_{t-\delta/2}^{t+\delta/2} \exp\{j\Delta\theta(\tau, f)\}\, d\tau\right|$$

also referred to as smoothed phase-locking index (S-PLI), where averaging of the phase vectors proceeds over adjacent time points. Time smoothing diminishes the temporal resolution of the S-PLI measure. As with wavelet coherence, the width of the smoothing window should be adapted to the target frequency, and to the expected length of the coherent epochs. Surrogate data for a statistical test can be obtained by data

scrambling, that is, by the permutation of the temporal order of the samples in each of the two signals. For a review of surrogate data methods, see Paluš (1997) and Schreiber and Schmitz (2000).

Conclusion

We reviewed the nature of oscillations in human EEG and how to analyze them via wavelet analysis. We hope that we were able to convince the reader that oscillations are a valuable approach for looking at electrophysiological data that compliments the derivation of ERP signals. Our attempt to name a few of the many experiments investigating oscillations in the human EEG was by no means complete. However, the list gives a short overview of the different frequency bands and may give the interested reader a link to further articles. In addition to the frequency bands that we explicitly mentioned here, there are various others, ranging from oscillations close to 0 Hz up to 600 Hz (Curio, 1999).

We also hope that the reader has learned new ways to investigate oscillatory activity in EEG data. At the same time, we tried to show the limitations and caveats of the introduced methods. Wavelets are certainly not the only way to analyze oscillations, but they do have critical advantages over other methods. The possibility of investigating the time course of an oscillation and to compute time-frequency representations with variable resolutions are among the strengths of wavelet analysis, along with the analysis of phases and their temporal characteristics. However, one must take care with some of the analysis parameters, such as the number of cycles that determines the frequency resolution, as well as the temporal resolution of the analysis.

The interpretation of significant synchronies between brain signals that have been detected is not straightforward. Especially when dealing with EEG scalp recordings, spurious synchronies may arise from volume conduction and/or reference effects. Volume conduction leads to an artificially high synchrony, especially between adjacent electrodes because their recorded neuronal populations overlap in space (Srinivasan, Nunez, & Silberstein, 1998). The effect of the choice of a specific reference electrode can hardly be predicted without precise knowledge of the source locations and of the volume conductor (Nunez et al., 1997). It may lead to an increase as well as to a decrease of measured synchrony between EEG recordings due to adding or removing a common signal, respectively. To circumvent these problems, one can enhance the spatial resolution of EEG recordings by deblurring techniques (Le & Gevins, 1993), scalp current density (SCD) calculation (Pernier, Perrin, & Bertrand, 1988; Lagerlund et al., 1995), or cortical imaging (Nunez et al., 1994) prior to wavelet analysis. However, Biggins et al. (1991) argued that SCD estimation could also introduce spurious synchronies due to spatial interpolation inherent in the mathematical algorithm. A

challenging approach could be to combine inverse methods and TF methods in order to reconstruct the sources of oscillatory neuroelectrical activity.

Of course, the approaches we focused on are not the only ones. There are a number of other fruitful applications of wavelets in neurophysiology, and some of them will probably gain more importance in the future.

One approach that is very promising is using a discrete wavelet analysis for denoising. An averaged ERP may be decomposed into wavelet coefficients by a discrete wavelet analysis. Then one can determine which coefficients yield significant activity at the corresponding frequency. In a second step only these significant coefficients are considered and others are set to zero. Now the ERP is reconstructed from the remaining wavelet coefficients. This procedure results in filtering out other frequencies that are considered noise for the cognitive task (e.g., Wang, Begleiter, & Pojesz, 1998; Quiroga & Garcia, 2003).

References

Adrian, E. (1942). Olfactory reactions in the brain of the hedgehog. *Journal of Physiology (London), 100,* 459–473.

Başar, E., Başar-Eroglu, C., Karakas, S., & Schürmann, M. (1999). Oscillatory brain theory: A new trend in neuroscience. *IEEE Engineering in Medicine and Biology, 18,* 56–66.

Başar, E., Schürmann, M., Başar-Eroglu, C., & Karakas, S. (1997). Alpha oscillations in brain functioning: An integrative theory. *International Journal of Psychophysiology, 26* (1–3), 5–29.

Başar-Eroglu, C., Strüber, D., Schürmann, M., Stadler, M., & Başar, E., (1996). Gamma-band responses in the brain: A short review of psychophysiological correlates and functional significance. *International Journal of Psychophysiology, 24,* 101–112.

Başar-Eroglu, C., Başar, E., Demiralp, T., & Schürmann, M. (1992). P300-response: Possible psychophysiological correlates in delta and theta frequency channels. A review. *International Journal of Psychophysiology, 13* (2), 161–179.

Biggins, C. A., Fein, G., Raz, J., & Amir, A. (1991). Artifactually high coherences result from using spherical spline computation of scalp current density. *Electroencephalography and Clinical Neurophysiology, 79,* 413–419.

Böttger, D., Herrmann, C. S., & von Cramon, D. Y. (2002). Amplitude differences of evoked alpha and gamma oscillations in two different age groups. *International Journal of Psychophysiology, 45* (3), 245–251.

Brandt, M. E. (1997). Visual and auditory evoked phase resetting of the alpha EEG. *International Journal of Psychophysiology, 26* (1–3), 319–340.

Berger, H. (1929). Über das Elektrenkephalogramm des Menschen. *Archiv für Psychiatrie und Nervenkrankheiten, 87,* 527–570.

Bruns, A., Eckhorn, R., Jokeit, H., & Ebner, A. (2000). Amplitude envelope correlation detects coupling among incoherent brain signals. *Cognitive Neuroscience, 11* (7), 1509–1514.

Chen, A. C. N., & Herrmann, C. S. (2001). Perception of pain coincides with the spatial expansion of human EEG dynamics. *Neuroscience Letters, 297* (3), 183–186.

Curio, G. (1999). High frequency (600 Hz) bursts of spike-like activities generated in the human cerebral somatosensory system. *Electroencephalography and Clinical Neurophysiology, 49,* 56–61.

Debener, S., Herrmann, C. S., Kranczioch, C., Gembris, D., & Engel, A. K. (2003). Top-down attentional processing enhances auditory evoked gamma band activity. *Neuroreport, 14* (5), 683–686.

Dumermuth, G. (1977). Fundamentals of spectral analysis in electroencephalography. In A. Remond (Ed.), *EEG informatics. A didactic review of methods and applications of EEG data processing* (pp. 83–105). Amsterdam: Elsevier.

Eckhorn, R., Bauer, R., Jordan, W., Brosch, M., Kruse, W., Munk, M., & Reitboeck, H. J. (1988). Coherent oscillations: A mechanisms of feature linking in the visual cortex? Multiple electrode and correlation analyses in the cat. *Biological Cybernetics, 60,* 121–130.

Engel, A. K., Fries, P., & Singer, W. (2001). Dynamic predictions: Oscillations and synchrony in top-down processing. *Nature Reviews Neuroscience, 2* (10), 704–716.

Fell, J., Klaver, P., Elfadil, H., Schaller, C., Elger, C. E., & Fernandez, G. (2003). *European Journal of Neuroscience, 17* (5), 1082–1088.

Fell, J., Klaver, P., Lehnertz, K., Grunwald, T., Schaller, C., Elger, C. E., & Fernandez, G. (2001). Human memory formation is accompanied by rhinal-hippocampak coupling and decoupling. *Nature Neuroscience, 4,* 1259–1264.

Gabor, D. (1946). Theory of communication. *Journal of IEE London, 93* (3), 429–457.

Galambos, R. (1992). A comparison of certain gamma band (40 Hz) brain rhythms in cat and man. In E. Başar & T. Bullock (Eds.), *Induced rhythms in the brain* (pp. 201–216). Boston: Birkhauser.

Gloor, P., Ball, G., & Schaul, N. (1977). Brain lesions that produce delta waves in the EEG. *Neurology, 27* (4), 326–333.

Gray, C. M., König, P., Engel, A. K., & Singer, W. (1989). Oscillatory responses in cat visual cortex exhibit intercolumnar synchronization which reflects global stimulus properties. *Nature, 338,* 334–337.

Haenschel, C., Baldeweg, T., Croft, R. J., Whittington, M., & Gruzelier, J. (2000). Gamma and beta frequency oscillations in response to novel auditory stimuli: A comparison of human electroencephalogram (EEG) data with in vitro models. *Proceedings of the National Academy of Sciences USA, 97* (13), 7645–7650.

Herrmann, C. S. (2001). Human EEG responses to 1–100 Hz flicker: Resonance phenomena in visual cortex and their potential correlation to cognitive phenomena. *Experimental Brain Research, 137,* 346–353.

Herrmann, C. S., & Knight, R. T. (2001). Mechanisms of human attention: Event-related potentials and oscillations. *Neuroscience and Biobehavioural Systems, 25* (6), 465–476.

Herrmann, C. S., & Mecklinger, A. (2001). Gamma activity in human EEG reflects attentional top-down processing. *Visual Cognition, 8*, 273–285.

Herrmann, C. S., Mecklinger, A., & Pfeiffer, E. (1999). Gamma responses and ERPs in a visual classification task. *Clinical Neurophysiology, 110*, 636–642.

Jensen, O., & Tesche, C. D. (2002). Frontal theta activity in humans increases with memory load in a working memory task. *European Journal of Neuroscience, 15* (8), 1395–1399.

Keil, A., Müller, M. M., Ray, W., Gruber, T., & Elbert, T. (1999). Human gamma band activity and perception of a gestalt. *The Journal of Neuroscience, 19*, 7152–7162.

Klimesch, W., Doppelmayr, M., Russegger, H., Pachinger, T., & Schwaiger, J. (1998a). Induced alpha band power changes in the human EEG and attention. *Neuroscience Letters, 13*, 73–76.

Klimesch, W., Doppelmayr, M., Rohm, D., Pollhuber, D., & Stadler, W. (1998b). Simultaneous desynchronization and synchronization of different alpha responses in the human electroencephalogram: A neglected paradox? *Neurocience Letters, 244*, 73–76.

Klimesch, W. (1997). EEG-alpha rhythms and memory processes. *International Journal of Psychophysiology, 26* (1–3), 319–340.

Klimesch, W., Schimke, H., & Pfurtscheller, G. (1993). Alpha frequency, cognitive load and memory performance. *Brain Topography, 5* (3), 241–251.

Lachaux, J.-P., Rodriguez, E., Martinerie, J., & Varela, F. J. (1999). Measuring phase synchrony in brain signals. *Human Brain Mapping, 8*, 194–208.

Lachaux, J.-P., Rodriguez, E., Le Van Quyen, M., Lutz, A., Martinerie, J., & Varela, F. J. (2000). Studying single-trials of phase synchronous activity in the brain. *International Journal of Bifurcation and Chaos, 10* (10), 2429–2439.

Lachaux, J.-P., Lutz, A., Rudrauf, D., Cosmelli, D., Le Van Quyen, M., Martinerie, J., & Varela, F. (2002). Estimating the time-course of coherence between single-trial brain signals: An introduction to wavelet coherence. *Neurophysiologie Clinique, 32*, 157–174.

Lagerlund, T. D., Sharbrough, F. W., Busacker, N. E., & Cicora, K. M. (1995). Interelectrode coherences from nearest-neighbor and spherical harmonic expansion computation of laplacian scalp potential. *Electroencephalography and Clinical Neurophysiology, 95*, 178–188.

Le, J., & Gevins, A. (1993). Methods to reduce blur distortion from EEGs using a realistic head model. *IEEE Transactions on Biomedical Engineering, 40*, 517–528.

Llinás, R., & Ribary, U. (1993). Coherent 40-Hz oscillation characterizes dream state in humans. *Proceedings of the National Academy of Sciences USA, 90* (5), 2078–2081.

Lopes da Silva, F. (1991). Neural mechanisms underlying brain waves: From neural membranes to networks. *Electroencephalography and Clinical Neurophysiology, 79* (2), 81–93.

Makeig, S., Westerfield, M., Jung, T. P., Enghoff, S., Townsend, J., Courchesne, E., & Sejnowski, T. J. (2002). Dynamic brain sources of visual evoked responses. *Science, 295*, 690–694.

Mardia, K. V., & Jupp, P. E. (2000). *Directional statistics*. Chichester: John Wiley & Sons Ltd.

Müller, M. M., Junghöfer, M., Elbert, T., & Rockstroh, B. (1997). Visually induced gamma-band responses to coherent and incoherent motion: A replication study. *NeuroReport, 8*, 2575–2579.

Müller, M. M., Teder-Sälejärvi, W., & Hillyard, S. (1998). The time course of cortical facilitation during cued shifts of spatial attention. *Nature Neuroscience, 1*, 631–634.

Müller, M. M., Gruber, T., Keil, A., & Elbert, T. (2000). Modulation of induced gamma band activity in the human EEG by attention and visual processing. *International Journal of Psychophysiology, 38*, 283–299.

Neuper, C., & Pfurtscheller, G. (2001). Event-related dynamics of cortical rhythms: Frequency-specific features and functional correlates. *International Journal of Psychophysiology, 43*, 41–58.

Niedermeyer, E. (1997). Alpha rhythms as physiological and abnormal phenomena. *International Journal of Psychophysiology, 26* (1–3), 31–49.

Nunez, P. L., Silberstein, R. B., Cadusch, P. J., Wijesinghe, R. S., Westdorp, A. F., & Srinivasan, R. (1994). A theoretical and experimental study of high resolution EEG based on surface Laplacians and cortical imaging. *Electroencephalography and Clinical Neurophysiology, 90*, 40–57.

Nunez, P. L., Srinivasan, R., Westdorp, A. F., Wijesinghe, R. S., Tucker, D. M., Silberstein, R. B., & Cadusch, P. J. (1997). EEG coherency I: Statistics, reference electrode, volume conduction, Laplacians, cortical imaging, and interpolation at multiple scales. *Electroencephalography and Clinical Neurophysiology, 103*, 499–515.

Paluš, M. (1997). Detecting phase synchronization in noisy systems. *Physics Letters A, 235*, 341–351.

Pernier, J., Perrin, F., & Bertrand, O. (1988). Scalp current densities: Concept and properties. *Electroencephalography and Clinical Neurophysiology, 69*, 385–389.

Polich, J. (1997). EEG and ERP assessment of normal aging. *Electroencephalography and Clinical Neurophysiology, 104*, 224–256.

Quiroga, R. Q., & Garcia, H. (2003). Single-trial event-related potentials with wavelet denoising. *Clinical Neurophysiology, 114*, 376–390.

Rappelsberger, P., Pfurtscheller, G., & Filz, O. (1994). Calculation of event-related coherence—a new method to study short-lasting coupling between brain areas. *Brain Topography, 7*, 121–127.

Rodriguez, E., George, N., Lachaux, J.-P., Martinerie, J., Renault, B., & Varela, F. J. (1999). Perception's shadow: Long-distance synchronization of human brain activity. *Nature, 397*, 430–433.

Roelfsema, P. R., Engel, A. K., König, P., & Singer, W. (1997). Visuomotor integration is associated with zero time-lag synchronization among cortical areas. *Nature, 385*, 157–161.

Rosenblum, M., Pikovsky, A., & Kurths, J. (1996). Phase synchronization of chaotic oscillators. *Physical Review Letters, 76*, 1804–1807.

Rosenblum, M., Pikovsky, A., Kurths, J., Schaefer, C., & Tass, P. A. (2001). Phase synchronization: From theory to data analysis. In F. Moss & S. Gielen (Ed.), *Handbook of biological physics, volume 4* (pp. 279–231). Elsevier Science.

Salmelin, R., & Hari, R. (1994). Spatiotemporal characteristics of sensorimotor neuromagnetic rhythms related to thumb movement. *Neuroscience, 60*, 537–550.

Samar, V. J., Bopardikar, A., Rao, R., & Swartz, K. (1999). Wavelet analysis of neuroelectric waveforms. *Brain and Language, 66*, 7–60.

Sewards, T. V., & Sewards, M. A. (1999). Alpha-band oscillations in visual cortex: Part of the neural correlate of visual awareness? *International Journal of Psychophysiology, 33* (2), 177–179.

Schack, B., Chen, A. C. N., Mescha, S., & Witte, H. (1999). Instantaneous EEG coherence analysis during the Stroop task. *Clinical Neurophysiology, 110*, 1410–1426.

Schiff, S. J., Aldroubi, A., Unser, M., & Sato, S. (1994). Fast wavelet transformation of EEG. *Electroencephalography and Clinical Neurophysiology, 91* (6), 442–455.

Schreiber, T., & Schmitz, A. (2000). Surrogate time series. *Physica D, 142*, 346–382.

Srinivasan, R., Nunez, P. L., & Silberstein, R. B. (1998). Spatial filtering and neocortical dynamics: Estimates of EEG coherence. *IEEE Transactions on Biomedical Engineering, 45*, 814–826.

Steriade, M., McCormick, D. A., & Sejnowski, T. J. (1993). Thalamo-cortical oscillations in the sleeping and aroused brain. *Science, 262*, 679–685.

Steriade, M., Gloor, P., Llinás, R., Lopes da Silva, F., & Mesulam, M. (1990). Basic mechanisms of cerebral rhythmic activities. *Electroencephalography and Clinical Neurophysiology, 76* (6), 481–508.

Strüber, D., & Herrmann, C. S. (2002). MEG alpha activity decrease reflects destabilization of multistable percepts. *Cognitive Brain Research, 14* (3), 370–382.

Tallon, C., Bertrand, O., Bouchet, P., & Pernier, J. (1995). Gamma range activity evoked by coherent visual stimuli in humans. *European Journal of Neuroscience, 7*, 1285–1291.

Tallon-Baudry, C., Bertrand, O., & Fischer, C. (2001). Oscillatory synchrony between human extrastriate areas during visual short-term memory maintenance. *Journal of Neuroscience, 21*, 1–5.

Tallon-Baudry, C., & Bertrand, O. (1999). Oscillatory gamma activity in humans and its role in object representation. *Trends in Cognitive Sciences, 3*, 151–162.

Tallon-Baudry, C., Bertrand, O., Delpuech, C., & Pernier, J. (1996). Stimulus specificity of phase-locked and non-phase-locked 40 Hz visual responses in human. *Journal of Neuroscience, 16*, 4240–4249.

Tallon-Baudry, C., Bertrand, O., Delpuech, C., & Pernier, J. (1997). Oscillatory gamma-band (30–70 Hz) activity induced by a visual search task in humans. *Journal of Neuroscience, 17*, 722–734.

Tass, P., Rosenblum, M. G., Weule, J., Kueths, J., Pikovsky, A., Volkmann, J., Schnitzler, A., & Freund, H. J. (1998). Detection of n:m phase locking from noisy data: Application to magnetoencephalography. *Physical Review Letters, 81*, 3291–3294.

Tesche, C. D., & Karhu, J. (2000). Theta oscillations index human hippocampal activation during a working memory task. *Proceedings of the National Academy of Sciences USA, 97* (2), 919–924.

Theiler, J., Eubank, S., Longtin, A., Galdrikian, B., & Farmer, J. D. (1992). Testing for nonlinearity in time series: The method of surrogate data. *Physica D, 58*, 77–94.

Tiitinen, H., Sinkkonen, J., Reinikainen, K., Alho, K., Lavikainen, J., & Näätänen, R. (1993). Selective attention enhances the auditory 40-hz transient response in humans. *Nature, 364*, 59–60.

Varela, F., Lachaux, J.-P., Rodriguez, E., & Martinerie, J. (2001). The brainweb: Phase synchronization and large-scale integration. *Nature Reviews Neuroscience, 2*, 229–239.

von Stein, A., Rappelsberger, P., Sarnthein, J., & Petsche, H. (1999). Synchronization between temporal and parietal cortex during multimodal object processing in man. *Cerebral Cortex, 9* (2), 689–692.

Wang, K., Begleiter, H., & Pojesz, B. (1998). Spatial enhancement of event-related potentials using multiresolution analysis. *Brain Topography, 10* (3), 191–200.

Welch, P. D. (1967). The use of fast Fourier transform for the estimation of power spectra: A method based on time averaging over short, modified periodograms. *IEEE Transactions Audio Electroacoustic, AU-15*, 70–73.

Yordanova, J., Kolev, V., & Polich, J. (2001). P300 and alpha event-related desynchronization (ERD). *Psychophysiology, 38*, 143–152.